Dalton Transactions

RSC Publishing

PAPER

View Article Online
View Journal | View Issue

Thermoelectric properties of Zn-doped $Ca_5In_2Sb_6$

Cite this: *Dalton Trans.*, 2013, **42**, 9713

Alex Zevalkink, Jessica Swallow and G. Jeffrey Snyder*

The Zintl compound $Ca_5Al_2Sb_6$ is a promising thermoelectric material with exceptionally low lattice thermal conductivity resulting from its complex crystal structure. In common with the Al analogue, $Ca_5In_2Sb_6$ is naturally an intrinsic semiconductor with a low p-type carrier concentration. Here, we improve the thermoelectric properties of $Ca_5In_2Sb_6$ by substituting Zn^{2+} on the In^{3+} site. With increasing Zn substitution, the $Ca_5In_{2-x}Zn_xSb_6$ system exhibits increased p-type carrier concentration and a resulting transition from non-degenerate to degenerate semiconducting behavior. A single parabolic band model was used to estimate an effective mass in $Ca_5In_2Sb_6$ of $m^* = 2m_e$, which is comparable to the Al analogue, in good agreement with density functional calculations. Doping with Zn enables rational optimization of the electronic transport properties and increased zT in accordance with a single parabolic band model. The maximum figure of merit obtained in optimally Zn-doped $Ca_5In_2Sb_6$ is 0.7 at 1000 K. While undoped $Ca_5In_2Sb_6$ has both improved electronic mobility and reduced lattice thermal conductivity relative to $Ca_5Al_2Sb_6$, these benefits did not dramatically improve the Zn-doped samples, leading to only a modest increase in zT relative to optimally doped $Ca_5Al_2Sb_6$.

Received 14th February 2013,
Accepted 22nd April 2013

DOI: 10.1039/c3dt50428j

www.rsc.org/dalton

Introduction

Thermoelectric materials convert heat directly to electricity, enabling solid state devices that can be used in applications ranging from industrial waste-heat recovery to long-term power generation on deep-space missions.[1] The widespread use of such devices is limited by the efficiency of thermoelectric materials, which is determined by their figure of merit, or zT ($zT = \frac{\alpha^2 T}{\rho(\kappa_e+\kappa_L)}$). High performance thermoelectric materials must achieve an optimum balance between the interdependent Seebeck coefficient (α), electrical resistivity (ρ), and electronic contribution to the thermal conductivity (κ_e).[2] The lattice thermal conductivity, κ_L, can often be engineered independently, making the reduction of κ_L a frequently used strategy in thermoelectric research.[3]

Zintl compounds have emerged as promising candidates for thermoelectric applications due to their rich chemistry and exceptionally low lattice thermal conductivity.[4] In the past decade, many complex Zintl phases with desirable thermal properties have been identified as promising thermoelectric materials.[5–9] The prevalence of complex crystal structures in Zintl compounds arises from their characteristic combination of covalently-bonded, anionic structures, and the surrounding ionically-bonded cations.[10,11] Such complexity results in glass-like lattice thermal conductivity at high temperatures, due to confinement of heat in low velocity, optical phonon modes, as well as additional opportunities for scattering events.[12–14] This is demonstrated by the compounds $Yb_{14}AlSb_{11}$ and Sr_3GaSb_3, both of which exhibit extremely low lattice thermal conductivity (~0.4 W mK^{-1}) owing to their large unit cells (104 and 54 atoms per unit cell, respectively).[7,15] Complexity in Zintl compounds also leads to many available sites for doping or isoelectronic substitutions, and thus to extensive opportunities to tune transport properties.[15,16]

Recently, several Zintl compounds with the structure type $Ca_5Ga_2As_6$ have been the focus of both experimental and computational studies.[17–19] $A_5M_2Pn_6$ compounds with the $Ca_5Ga_2As_6$ structure type are characterized by chains of corner-linked MPn_4 tetrahedra, which are connected by Pn–Pn dimers to form infinite, ladder-like structures, as shown in Fig. 1a

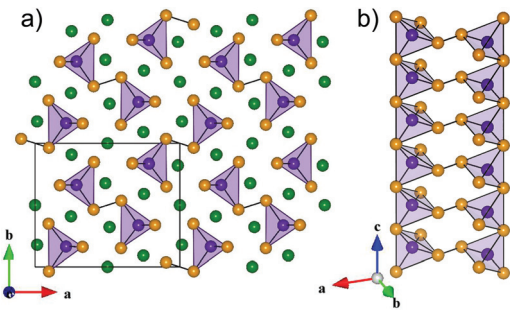

Fig. 1 (a) The crystal structure of $Ca_5In_2Sb_6$ (orthorhombic, *Pbam*) viewed down the chains of corner-sharing $InSb_4$ tetrahedra. (b) Adjacent chains are connected *via* covalent Sb–Sb bonds, resulting in ladder-like moieties. Ca atoms are shown in green, Sb in orange, and In in purple.[28]

Materials Science, California Institute of Technology, 1200 E. California Blvd., Pasadena, CA 91125, USA. E-mail: jsnyder@caltech.edu

and b.[20] The Zintl concept is satisfied as follows: the M atoms are 4-bonded with a formal charge of 1−. Two Pn^{1-} form the ladder "rungs", two additional Pn^{1-} atoms are bonded to two M atoms, and two Pn^{2-} are bonded only to one M atom. The five A^{2+} cations surrounding the ladders lead to overall charge balance. In these compounds, the alkaline earth site (A) can accept Ca, Sr or Ba, while the M site accepts Al, Ga, or In. The pnictogen site can be filled by As or Sb. One rare-earth based compound, $Eu_5In_2Sb_6$, has also been reported, and appears to be a narrow-band gap semiconductor.[21] The substitution of Yb on the cation site leads to the formation of a closely related crystal structure based on an alternate packing arrangement of the anionic "ladders" (structure type $Ba_5Al_2Bi_6$).[22,23]

Our initial investigation of $Ca_5Al_2Sb_6$ revealed extremely low lattice thermal conductivity, approaching the amorphous limit at high temperatures (0.6 W mK^{-1} at 1000 K). This, combined with a large band gap (~0.6 eV) and successful doping, resulted in a peak zT of 0.6 at 1000 K.[17] We recently investigated trends in the chemical and transport properties of the $Ca_5M_2Sb_6$ system (M = Al, Ga, and In), the results of which suggested potential routes towards improved thermoelectric performance in this system.[19] Relative to $Ca_5Al_2Sb_6$, the In- and Ga-based compounds exhibited improvements to both electronic and thermal properties; the lattice thermal conductivity was reduced due to higher density and reduced stiffness, which in turn decreases the speed of sound ($\nu \propto \sqrt{E/d}$, where E is stiffness and d is density), and the electronic mobility was improved. In contrast to $Ca_5Ga_2Sb_6$, which had a significantly reduced band gap relative the Al analogue and thus reduced performance at high temperatures,[24] the band gap of $Ca_5In_2Sb_6$ is very similar to that of the Al analogue. Upon optimization of the carrier concentration through doping, $Ca_5In_2Sb_6$ is thus expected to have an improved peak zT relative to both $Ca_5Al_2Sb_6$ and $Ca_5Ga_2Sb_6$.

The current study investigates the electronic and thermal properties of $Ca_5In_{2-x}Zn_xSb_6$ (x = 0, 0.02, 0.05, 0.1, 0.2). Zn^{2+} acts as a p-type dopant on the In^{3+} site in the otherwise charge-balanced $Ca_5In_2Sb_6$, allowing the study of samples with a wide range of carrier concentrations. We use solutions to the Boltzmann transport equation, assuming rigid, single parabolic band behavior to analyze transport data and to guide in the optimization of the carrier concentration and the figure of merit.

Experimental

Synthesis

InSb was formed as a precursor by melting 99.999% In shot from Alpha Aesar and 99.5% Sb lumps from Sigma-Aldrich in vacuum sealed, carbon-coated quartz ampoules at 973 K for 10 h, and then quenching in water. Stoichiometric amounts of the crushed InSb precursor, 99.99% Ca dendrites, 99.99% Zn shot, and 99.5% Sb lumps from Sigma-Aldrich were loaded into stainless-steel vials with stainless-steel balls in an argon-filled glove box. The contents were dry ball-milled for 1 h using a SPEX Sample Prep 8000 Series Mixer/Mill. The resulting fine powder was hot-pressed in high-density graphite dies (POCO) in argon using 110 MPa of pressure. Before applying pressure, samples were held for 2 h at 723 K to ensure complete reaction of any remaining InSb, then consolidated for 3 h at 973 K, followed by a 3 h stress-free cool down.

Characterization

Hot-pressed, polycrystalline samples were sliced into 1 mm thick, 12 mm diameter disks. X-Ray diffraction was performed on polished slices using a Philips XPERT MPD diffractometer operated at 45 kV and 40 mA, and Rietveld analysis was performed using Philips X'Pert Plus software. Scanning electron microscopy and energy dispersive spectroscopy were performed using a Zeiss 1550 VP SEM. High temperature electronic properties were characterized to 973 K under dynamic vacuum. Electrical resistivity was determined using the van der Pauw technique and the Hall coefficient was measured with a 2 T field and pressure-assisted contacts.[25] The Seebeck coefficients of the samples in this study as well as the $Ca_{5-x}Na_x$-Al_2Sb_6 samples from ref. 17 were measured using W–Nb thermocouples by allowing the temperature gradient across the sample to oscillate between ±10 K.[27] For the samples in ref. 24 and 29, an alternate setup with chromel–Nb thermocouples was used to measure the Seebeck coefficient, as described in ref. 26. A Netzsch LFA 457 was used to measure the thermal diffusivity.

Results and discussion

The phase purity of the hot-pressed $Ca_5In_{2-x}Zn_xSb_6$ (x = 0, 0.02, 0.05, 0.1, 0.2) samples was confirmed by X-ray diffraction (XRD) and scanning electron microscopy (SEM). Fig. 2 shows a representative XRD pattern, a Rietveld fit using the known crystal structure of $Ca_5In_2Sb_6$,[28] and the difference profile. From the XRD patterns, all of the samples in this study appear to be phase pure. However, an unidentified secondary phase is

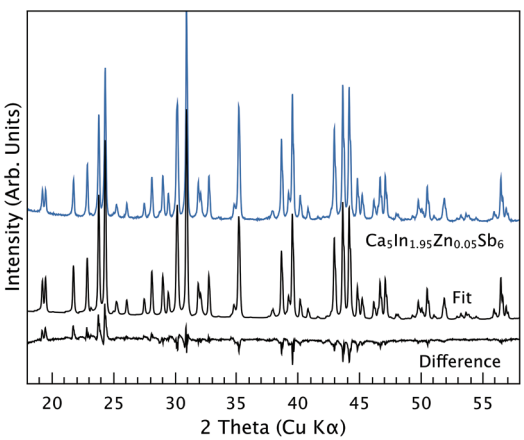

Fig. 2 XRD pattern of a polycrystalline slice of the x = 0.05 sample, Rietveld fit using the known $Ca_5In_2Sb_6$ structure, and difference profile.

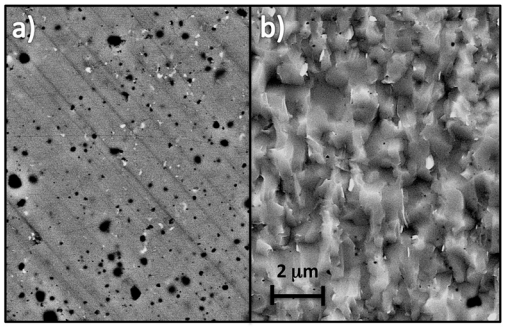

Fig. 3 (a) Backscattered electron image of a polished surface of $Ca_5In_{1.9}Zn_{0.1}Sb_6$ showing representative phase fractions of $Ca_5In_2Sb_6$ (grey), a secondary phase (light grey), and pores (black). (b) Secondary electron image of a fracture surface of the same sample reveals grain sizes on the order of 1 μm.

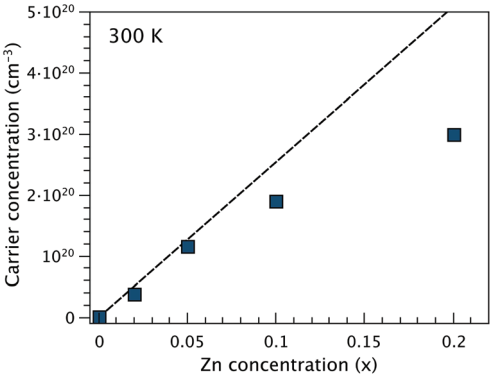

Fig. 4 With increasing Zn content, the Hall carrier concentration at 300 K in $Ca_5In_{2-x}Zn_xSb_6$ increases as predicted by simple charge counting (dashed line) up to $x = 0.05$.

visible as ~100 nm white flecks in the backscatter electron image in Fig. 3a. This impurity appears to make up less than 1 vol% of the sample, and is not expected to have a significant impact on transport properties. The lattice parameters obtained from Rietveld refinements suggest that the $Ca_5In_{2-x}Zn_xSb_6$ system is a solid solution up to only $x = 0.05$. The ionic radii of four-coordinated Zn and In are respectively 0.60 and 0.62 Å. As expected, with increasing Zn content, the unit cell volume was found to decrease. However, above $x = 0.05$ the volume remained constant. The light grey impurity observed in scanning electron microscopy (SEM) images appears in similar concentrations in all samples (both doped and undoped), and is therefore not likely to be due to the addition of Zn. However, given the low solubility of Zn in $Ca_5In_2Sb_6$, an additional, Zn-rich secondary phase is likely present in the samples with $x = 0.1$ and $x = 0.2$.

The samples' geometric densities range from 95–97% of the theoretical density (4.90 g cm^{-3}), consistent with the fraction of pores observed in SEM analysis. SEM images of fracture surfaces (Fig. 3b) reveal grain sizes on the order of a few microns. This is similar to Zn-doped $Ca_5Al_2Sb_6$ samples,[29] but small compared to Na-doped $Ca_5Al_2Sb_6$, which had average grains sizes of 50–100 μm.[17] Attempts to increase the grain size in $Ca_5In_2Sb_6$ by doubling the hot pressing time did not lead to an appreciable difference. Neither the density, grain size, nor phase purity appear to be a function of Zn concentration.

Electronic transport properties

$Ca_5In_2Sb_6$ is a classic, valence-precise Zintl compound, in common with the Al and Ga analogues of the same structure. In practice, nominally undoped $Ca_5In_2Sb_6$ samples were found to be lightly hole doped ($n = 5 \times 10^{18}$ h^+ cm^{-3}) at room temperature. The room temperature carrier concentrations were shown to be similar in all three $Ca_5M_2Sb_6$ compounds, suggesting that the M atom does not affect the equilibrium concentration of intrinsic crystalline defects.[19]

Upon doping, simple charge counting predicts that each Zn^{2+} on an In^{3+} site will lead to one free hole. The predicted relationship between carrier concentration (n) and x is shown as a dashed line in Fig. 4. At low doping levels, the measured Hall carrier concentration (n_H) increases according to the predicted trend, but n_H diverges downwards for $x > 0.05$ (Fig. 4). The reduced doping effectiveness above $x = 0.05$ is most likely a result of limited Zn solubility. This is qualitatively consistent with our XRD data, which suggests that $Ca_5In_{2-x}Zn_xSb_6$ is only a true solid solution up to $x = 0.05$. Note that the sample compositions used throughout the figures and discussion refer to the nominal synthetic starting composition, rather than to the exact composition of the matrix.

Shown in Fig. 5a, n_H in undoped $Ca_5In_2Sb_6$ increases strongly as a function of temperature due to activation of minority carriers across the band gap. This leads to the decrease in resistivity (ρ) with temperature characteristic of intrinsic semiconductors (Fig. 5b). As discussed in ref. 19 the discontinuity in the Hall and resistivity measurements at 725 K is due to a reversible phase transition, confirmed by DSC measurements in both undoped and doped $Ca_5In_2Sb_6$. With increasing Zn content, n_H in $Ca_5In_{2-x}Zn_xSb_6$ increases by nearly two orders of magnitude, and becomes less temperature dependent, as shown in Fig. 5a. Correspondingly, the resistivity decreases and the temperature dependence transitions from semiconducting to metallic. Shown for comparison, the carrier concentration of optimally doped $Ca_{4.75}Na_{0.25}Al_2Sb_6$ from ref. 17 is equivalent to that of $Ca_5In_{1.9}Zn_{0.1}Sb_6$. Note that doping with Zn in $Ca_5In_2Sb_6$ increases n more effectively than Na in $Ca_5Al_2Sb_6$. Higher doping effectiveness is the primary reason that Zn, rather than Na, was used as a dopant in this study.

The Hall mobility (μ_H), calculated from $\rho = 1/ne\mu_H$, is shown in Fig. 5c. In both doped and undoped $Ca_5In_{2-x}Zn_xSb_6$ samples, the temperature dependence of μ at high temperatures is consistent with acoustic phonon scattering ($\mu \propto T^{-\nu}$, where ν ranges from 1.5 to 2.5). At room temp, the mobility of undoped $Ca_5In_2Sb_6$ is nearly twice that of undoped $Ca_5Al_2Sb_6$ (see ref. 19). With increased Zn doping however, the mobility decreases rapidly. Comparing $Ca_5Al_2Sb_6$ and $Ca_5In_2Sb_6$ samples with the same carrier concentrations reveals that $Ca_5In_{2-x}Zn_xSb_6$ has slightly higher mobility than Na-doped $Ca_5Al_2Sb_6$. However, the improvement is not as strong as observed in the undoped samples.

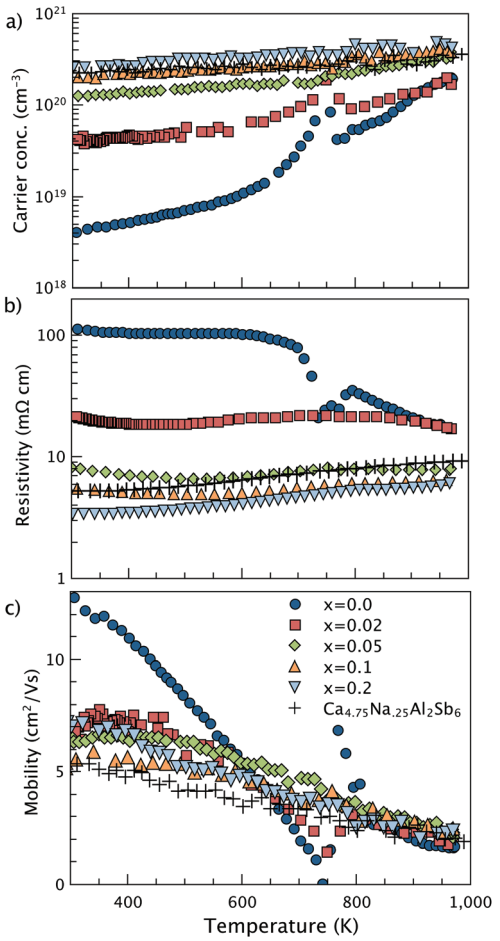

Fig. 5 (a) With increasing x in $Ca_5In_{2-x}Zn_xSb_6$, the carrier concentration increases and (b) the resistivity decreases by an order of magnitude. (c) The Hall mobility decreases with Zn content, becoming comparable to Na-doped $Ca_5Al_2Sb_6$ at high temperatures.

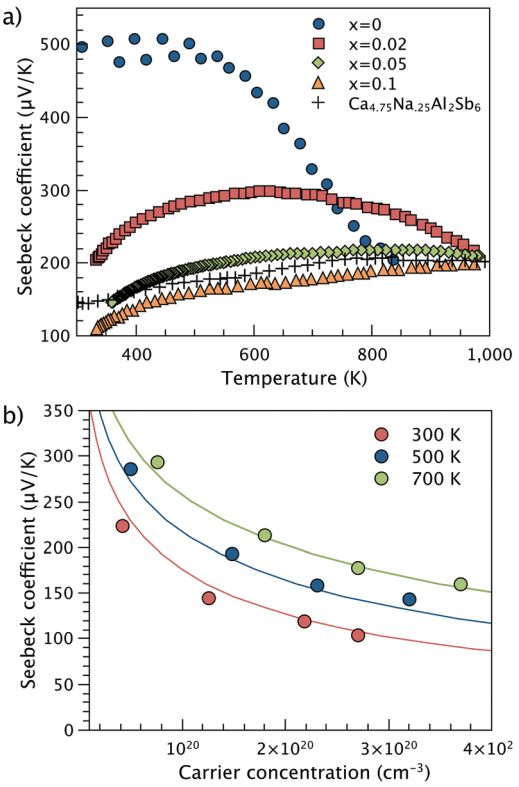

Fig. 6 (a) High temperature Seebeck coefficients of $Ca_5In_{2-x}Zn_xSb_6$ samples display increasingly linear behavior and decreased magnitude with increased Zn concentration. (b) Seebeck coefficients decrease as a function of n as predicted by a single parabolic band model (dashed curves). Effective masses of $2.0m_e$ (at 300 K and 500 K) and $1.8m_e$ (at 700 K) were calculated from the experimental α and n of the $x = 0.05$ sample.

$Ca_5In_2Sb_6$ has a large, positive Seebeck coefficient, which decreases with temperature due to thermally activated minority carriers (Fig. 6). With doping, the transition from non-degenerate to degenerate behavior leads to a decrease in the magnitude of the Seebeck coefficients, as well as a more linear temperature dependence. Due to their similar carrier concentrations, the samples $Ca_5In_{1.9}Zn_{0.1}Sb_6$ and $Ca_{4.75}Na_{0.25}Al_2Sb_6$ have comparable Seebeck coefficients.

In ref. 19, we reported a slight decrease in both the band gap and effective mass of $Ca_5In_2Sb_6$ relative to the Al analogue. This could be understood qualitatively in terms of the electronegativity difference between Al and In (1.61 and 1.78 respectively on the Pauling scale) and was supported by density functional calculations. While the influence of the modified electronic band structure was observed experimentally in undoped $Ca_5M_2Sb_6$ compounds, it does not appear to have a large influence on the electronic mobility and Seebeck coefficients of the doped samples.

Fig. 6 illustrates the dependence of the Seebeck coefficient on n_H, which is determined by the geometry of the valence band. The solid curves show the predicted dependence at selected temperatures, assuming a parabolic valence band edge. This model assumes that acoustic phonons are the dominant scattering source. A more complete description of this single parabolic band (SPB) model can be found in ref. 17 and 30. In $Ca_5M_2Sb_6$ compounds, the valence band edge is doubly degenerate at the Gamma point. A single band model approximates multi-band transport by fitting data to an "SPB" band mass (m^*_{SPB}). The "true" mass of each band (m^*_{band}) can be determined from $(m^*_{SPB})^{3/2} = N_v(m^*_{band})^{3/2}$ if the degeneracy (N_v) is known, and if the degenerate bands have equal mass.[31] The effective mass of $Ca_5In_2Sb_6$, as determined by an SPB model ($m^*_{SPB} = 2m_e$ at 300 and 500 K, and $1.8m_e$ at 700 K) is similar to that found in $Ca_5Al_2Sb_6$.

Thermal transport properties

The total thermal conductivity (κ) in a typical thermoelectric material is the sum of electronic (κ_e), bipolar (κ_B), and lattice (κ_L) contributions. At high temperatures, the lattice component generally decreases as $1/T$ due to Umklapp scattering, eventually approaching the minimum lattice thermal conductivity (κ_{min}) given by eqn (1).[32,33] This limit occurs when the phonon mean free path reaches $l = \lambda/2$, the smallest physically meaningful l for a phonon of wavelength λ. Here, V is the atomic

volume and ν_S and ν_L are respectively the transverse and longitudinal speed of sound.

$$\kappa_{min} = \frac{1}{2}\left(\frac{\pi}{6}\right)^{1/3} k_B V^{-2/3}(2\nu_S + \nu_L) \quad (1)$$

Due primarily to the complexity of its unit cell (26 atoms per cell), the lattice thermal conductivity in $Ca_5Al_2Sb_6$ was found to approach κ_{min} at the temperature corresponding to its maximum zT (~1000 K).[12,13] While nanostructuring or point defect scattering may further reduce κ_L at low temperatures, such strategies are not expected to reduce the high temp κ_L beyond the limit of eqn (1). One potential route to further reductions in κ_L at high temperature is to reduce κ_{min} itself, which can be accomplished by lowering the speed of sound.

The speed of sound in a solid increases with stiffness and decreases with density according to eqn (2) and (3). The substitution of In for Al in $Ca_5M_2Sb_6$ led to a 10% reduction in the speed of sound due to both increased density and decreased stiffness.[19]

	d (g cm^{-2})	G (GPa)	K (GPa)	ν_S (m s^{-1})	ν_L (m s^{-1})
$Ca_5In_2Sb_6$	4.90	22	38	2115	3710
$Ca_5Al_2Sb_6$	4.31	26	41	2440	4170

$$\nu_S = \sqrt{\frac{G}{d}} \quad (2)$$

$$\nu_L = \sqrt{\frac{K + \frac{4}{3}G}{d}} \quad (3)$$

The thermal conductivity (Fig. 7a) was calculated from the thermal diffusivity (D) according to $\kappa = C_p D d$, where in this case d is the geometric density, and C_p is the Dulong Petit heat capacity (0.279 J g^{-1} K^{-1}). Although it is common to use the Dulong Petit value at temperatures above θ_D, this can lead to an underestimate of the true C_p and therefore of the thermal conductivity, particularly at high temperatures. The electronic component of the thermal conductivity was estimated from the Wiedemann Franz relation ($\kappa_e = LT/\rho$), where the Lorenz number (L) was determined using the SPB model described in ref. 30 (inset in Fig. 7b). At temperatures beyond the onset of minority carrier activation, L was determined by extrapolation. Subtracting the electronic contribution from κ leaves both the lattice and bipolar terms, shown in Fig. 7b. In the undoped and lightly doped $Ca_5In_2Sb_6$, the bipolar term manifests itself as a rise in thermal conductivity at high temperatures. In the most heavily doped samples there is little evidence of a bipolar contribution. Despite the lower speed of sound in $Ca_5In_2Sb_6$, the lattice thermal conductivity of Zn-doped $Ca_5In_2Sb_6$ is comparable to that of Na-doped $Ca_5Al_2Sb_6$.

Figure of merit

The figure of merit of $Ca_5In_{2-x}Zn_xSb_6$ is shown as a function of temperature in Fig. 8, calculated from polynomial fits to the data. Doping with Zn leads to an increase from a maximum of

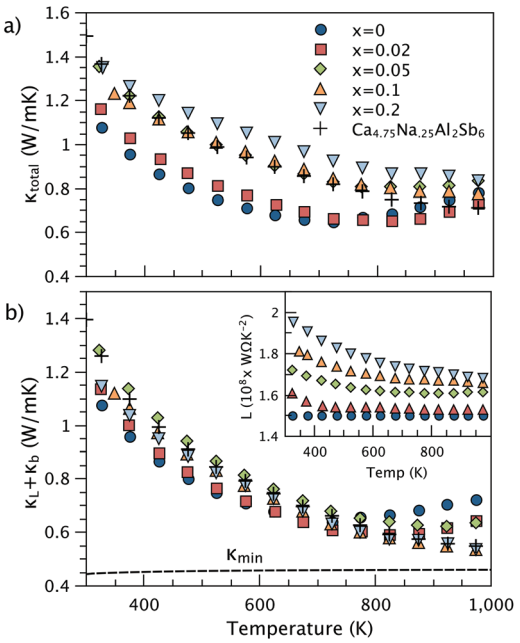

Fig. 7 (a) The total thermal conductivity and (b) the combined lattice and bipolar thermal conductivity of $Ca_5In_{2-x}Zn_xSb_6$. The inset shows the temperature dependence of the Lorenz numbers in units of 10^8 WΩ K^{-2}, calculated using an SPB model.

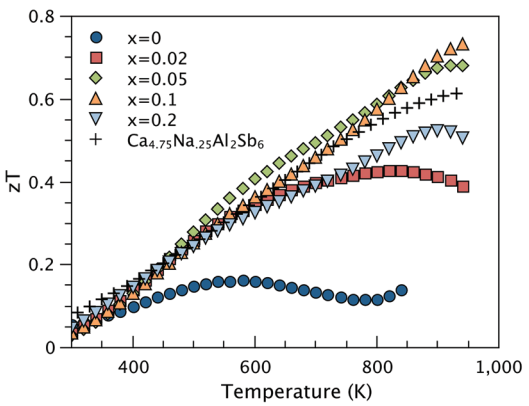

Fig. 8 The figure of merit of $Ca_5In_{2-x}Zn_xSb_6$ samples is comparable to Na-doped $Ca_5Al_2Sb_6$ within the measured temperature range.

zT = 0.15 in the undoped sample to a peak zT of approximately 0.7 in the x = 0.05 and x = 0.1 samples at 973 K. While the peak zT is also improved somewhat relative to the Al analogue, the difference is within the 20% measurement uncertainty in zT. To determine the optimal carrier concentrations required for maximum efficiency in $Ca_5In_2Sb_6$, the dependence of the Seebeck coefficient, mobility, and Lorenz number on n were calculated using the SPB model described above. From these, zT was calculated as a function of n at various temperatures, shown as solid curves in Fig. 9. This predicted optimum carrier concentration of 2 × 10^{20} cm^{-3} at high temperature is in agreement with our experimental results and suggests that further tuning of n is not necessary.

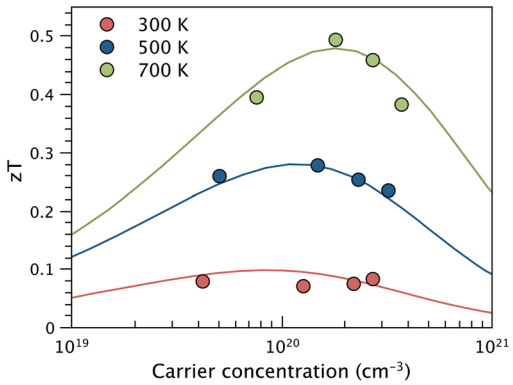

Fig. 9 The figure of merit at 700 K is optimized at 2×10^{20} cm^{-3}, in agreement with the SPB model. The parameters used at 300, 500 and 700 K, respectively were m^*_{SPB} = 2.0, 2.0, 1.8, κ_L = 1.2, 0.9, and 0.7 W mK^{-1}, and intrinsic mobilities of 7.6, 6.9, and 5.3 cm^2 Vs^{-1}.

Conclusion

Doping $Ca_5In_2Sb_6$ with Zn allows for rational control of the transition from non-degenerate to degenerate semiconducting behavior, providing a route to carrier concentration optimization in this material. Ultimately, a maximum zT of 0.7 was achieved at 950 K in optimally Zn-doped $Ca_5In_2Sb_6$. Although Zn-doped $Ca_5In_2Sb_6$ was expected to have higher mobility and lower lattice thermal conductivity than the Al analogue, the properties of the two systems were comparable within measurement uncertainty, leading to only a moderate improvement in the figure of merit.

Acknowledgements

We gratefully acknowledge the Jet Propulsion Laboratory and National Science Foundation for support. Jessica Swallow acknowledges the generous support of Marcella Bonsall for Caltech's Summer Undergraduate Research Program.

References

1 L. Bell, Cooling, heating, generating power, and recovering waste heat with thermoelectric systems, *Science*, 2008, **321**, 1457–1461.
2 G. J. Snyder and E. S. Toberer, Complex thermoelectric materials, *Nat. Mater.*, 2008, **7**, 105.
3 C. J. Vineis, A. Shakouri, A. Majumdar and M. G. Kanatzidis, Nanostructured thermoelectrics: big efficiency gains from small features, *Adv. Mater.*, 2010, **22**, 3970–3980.
4 E. S. Toberer, A. F. May and G. J. Snyder, Zintl chemistry for designing high efficiency thermoelectric materials, *Chem. Mater.*, 2010, **22**, 624–634.
5 E. S. Toberer, C. A. Cox, S. R. Brown, T. Ikeda, A. F. May, S. M. Kauzlarich and G. J. Snyder, Traversing the metal-insulator transition in a Zintl phase: rational enhancement of thermoelectric efficiency in $Yb_{14}Al_xMn_{1-x}Sb_{11}$, *Adv. Funct. Mater.*, 2008, **18**, 2795.
6 A. Zevalkink, E. S. Toberer, W. Zeier, E. Flage-Larsen and G. J. Snyder, Ca_3AlSb_3: an inexpensive, non-toxic thermoelectric material for waste heat recovery, *Energy Environ. Sci.*, 2011, **4**, 510–518.
7 A. Zevalkink, W. Zeier, G. S. Pomrehn, E. Schechtel and G. J. Snyder, Thermoelectric properties of Sr_3GaSb_3 – a chain-forming Zintl compound, *Energy Environ. Sci.*, 2012, **5**, 9121–9128.
8 J. Wang, S.-Q. Xia and X.-T. Tao, $A_5Sn_2As_6$ (A = Sr, Eu). Synthesis, crystal and electronic structure, and thermoelectric properties, *Inorg. Chem.*, 2012, **51**, 5771–5778.
9 S.-J. Kim and M. G. Kanatzidis, A unique framework in $BaGa_2Sb_2$: a new Zintl phase with large tunnels, *Inorg. Chem.*, 2001, **40**, 3781–3785.
10 S. M. Kauzlarich, *Chemistry, Structure, and Bonding of Zintl Phases and Ions*, Wiley-VCH, 1996.
11 A. M. Mills, R. Lam, M. J. Ferguson, L. Deakin and A. Mar, Chains, planes, and antimonides, *Coord. Chem. Rev.*, 2002, **223–234**, 207–222.
12 G. A. Slack, *Solid State Physics*, Academic Press, New York, 1979, vol. 34.
13 E. S. Toberer, A. Zevalkink and G. J. Snyder, Phonon engineering through crystal chemistry, *J. Mater. Chem.*, 2011, **21**, 15843–15852.
14 J. R. Sootsman, D. Y. Chung and M. G. Kanatzidis, New and old concepts in thermoelectric materials, *Angew. Chem., Int. Ed.*, 2009, **48**, 8616–8639.
15 C. A. Cox, E. S. Toberer, A. A. Levchenko, S. R. Brown, J. G. Snyder, A. Navrotsky and S. M. Kauzlarich, Structure, heat capacity, and high-temperature thermal properties of $Yb_{14}Mn_{1-x}Al_xSb_{11}$, *Chem. Mater.*, 2009, **21**, 1354–1360.
16 S. R. Brown, E. S. Toberer, T. Ikeda, F. Gascoin, S. M. Kauzlarich and J. G. Snyder, Improved thermoelectric performance in $Yb_{14}Mn_{1-x}Zn_xSb_{11}$ by the reduction of spin-disorder scattering, *Chem. Mater.*, 2008, **20**, 3412–3419.
17 E. S. Toberer, A. Zevalkink, N. Crisosto and G. J. Snyder, The Zintl compound $Ca_5Al_2Sb_6$ for low-cost thermoelectric power generation, *Adv. Funct. Mater.*, 2010, **20**, 4375–4380.
18 Y. L. Yan and Y. X. Wang, Crystal structure, electronic structure, and thermoelectric properties of $Ca_5Al_2Sb_6$, *J. Mater. Chem.*, 2011, **21**, 12497.
19 A. Zevalkink, G. S. Pomrehn, S. Johnson, J. Swallow, Z. M. Gibbs and G. J. Snyder, Influence of the triel elements (M = Al, Ga, In) on the transport properties of $Ca_5M_2Sb_6$ Zintl compounds, *Chem. Mater.*, 2011, **4**, 510–518.
20 G. Cordier, E. Czech, M. Jakowski and H. Schaefer, Zintl phases of complex ions – information on $Ca_5Al_2Sb_6$ and $Ca_3Al_2As_4$, *Rev. Chim. Miner.*, 1981, **18**, 9.
21 S. Park, E. Choi, W. Kang and S. Kim, $Eu_5In_2Sb_6$, $Eu_5In_{2-x}Zn_xSb_6$: rare earth zintl phases with narrow band gaps, *J. Mater. Chem.*, 2002, **12**, 1839–1843.
22 I. Todorov, D. Y. Chung, L. Ye, A. J. Freeman and M. G. Kanatzidis, Synthesis, structure and charge transport

properties of $Yb_5A_2Sb_6$: a Zintl phase with incomplete electron transfer, *Inorg. Chem.*, 2009, **48**, 4768–4776.

23 S.-J. Kim, J. R. Ireland, C. R. Kannewurf and M. G. Kanatzidis, $Yb_5In_2Sb_6$: a new rare earth Zintl phase with a narrow band gap, *J. Solid State Chem.*, 2000, **155**, 55–61.

24 S. Johnson, A. Zevalkink and G. J. Snyder, Improved thermoelectric properties in $Ca_5Ga_2Sb_6$, *J. Mater. Chem. A*, 2013, **1**, 4244–4249.

25 K. Borup, E. S. Toberer, L. D. Zoltan, G. Nakatsukasa, M. Errico, J.-P. Fleurrial, B. B. Iversen and G. J. Snyder, Measurement of the electrical resistivity and Hall coefficient at high temperatures, *Rev. Sci. Instrum.*, 2012, **83**, 123902.

26 S. Iwanaga, E. S. Toberer, A. Lalonde and G. J. Snyder, A high temperature apparatus for measurement of the Seebeck coefficient, *Rev. Sci. Instrum.*, 2011, **82**, 063905.

27 C. Wood, D. Zoltan and G. Stapfer, *Rev. Sci. Instrum.*, 1985, **56**, 719.

28 G. Cordier, H. Schaefer and M. Stelter, Perantimonidogallate und -indate: Zur Kenntnis von $Ca_5Ga_2Sb_6$, $Ca_5In_2Sb_6$ und $Sr_5In_2Sb_6$, *Z. Naturforsch., B: Anorg. Chem. Org. Chem.*, 1986, **33**, 5–8.

29 A. Zevalkink, E. S. Toberer, T. Bleith, E. Flage-Larsen and G. J. Snyder, Improved carrier concentration control in Zn-doped $Ca_5Al_2Sb_6$, *J. Appl. Phys.*, 2011, **110**, 013721.

30 A. F. May, E. S. Toberer, A. Saramat and G. J. Snyder, Characterization and analysis of thermoelectric transport in n-type $Ba_8Ga_{16-x}Ge_{30-x}$, *Phys. Rev. B: Condens. Matter*, 2009, **80**, 125205.

31 J. DiSalvo, Thermoelectric cooling and power generation, *Science*, 1999, **295**, 703.

32 D. G. Cahill and R. O. Pohl, Lattice vibrations and heat transport in crystals and glasses, *Annu. Rev. Phys. Chem.*, 1988, **39**, 93–121.

33 D. G. Cahill, S. K. Watson and R. O. Pohl, Lower limit to the thermal conductivity of disordered crystals, *Phys. Rev. B: Condens. Matter*, 1992, **46**, 6131–6140.